JOURNAL OF GUIDANCE, CONTROL, AND DYNAMICS
Vol. 31, No. 4, July–August 2008

Infinite-Horizon Control for Retrieving a Tethered Subsatellite via an Elastic Tether

Hao Wen,* Dongping Jin,† and Haiyan Hu‡
Nanjing University of Aeronautics and Astronautics, 210016 Nanjing, People's Republic of China

DOI: 10.2514/1.33224

This paper presents a nonlinear optimal control scheme for the retrieval of an elastically tethered subsatellite model. The scheme accounts for in-plane and out-of-plane motions. The control design is formulated over an infinite horizon by using a domain-transformation technique and all the nonlinearities in the system model are taken into consideration. Two Legendre pseudospectral algorithms are explored to find an optimal trajectory that guides the subsatellite from an initial position far from the spaceship into a final position close to the spaceship. The first approach involves direct transcription and nonlinear programming, and the second one is based on the method of quasi linearization and matrix algebra. The case studies in the paper well demonstrate the effectiveness and dominant real-time merits of the proposed strategies.

I. Introduction

THE concept of tethered satellite systems (that is, two or more satellites connected by thin and long cables) has found great value in space technology. Numerous important applications of such systems have been identified, ranging from propellantless propulsion for satellites, gravity gradient stabilization, tether-assisted reentry, and electrodynamic drives to power generation. Over the past decades, several successful projects [such as SEDS (Small Expendable Deployer System)] and partially successful projects (such as TSS-1) have been launched on NASA missions, as documented in [1].

Retrieval of a tethered subsatellite is one of the most important, but also the most delicate, stages of a tether mission. The main problem during the retrieval process is that the subsatellite, due to the effect of the Coriolis acceleration, does not move along a straight radial equilibrium configuration, which is stable for a tether of constant length moving on a circular orbit. Instead, an unstable motion around the radial equilibrium configuration may occur, especially at the end of the retrieval process. Because of their overall flexibility, the cables connecting satellites are strongly susceptible to undergoing a complicated set of coupled vibrations, such as the in-plane and out-of-plane librations and the longitudinal and transverse vibrations [2]. If not carefully controlled, the oscillatory motions during and after the retrieval may result in an excessively high tensional stress beyond the strength of tether material and may lead to the failure of the system. The modeling and analysis of such cablelike structures have attracted significant attention in the literature [3].

Optimal control may be ideal for the retrieval control problem, because the stringent performance requirements in a tether-retrieval scenario demand a level of accuracy that cannot be achieved by linearized feedback control. Furthermore, optimal control allows for accurate maneuvering of the system between the initial and terminal states. However, the classical closed-loop optimal control strategies are generally ill-suited for such problems, due to the difficulties in solving the associated Hamilton–Jacobi–Bellman equation, which is mainly attributed to the strong nonlinearity in the system dynamics. An alternative to solving the Hamilton–Jacobi–Bellman equation is to generate the optimal retrieval trajectory online. Nevertheless, it is not always easy to solve the open-loop optimal control problem efficiently and reliably for real-time implementation.

Over the past decades, significant research has been undertaken to study optimal control of tethered satellite systems. For example, Bainum and Kumar [4] analyzed the stability of a simplified model of a shuttle-subsatellite system and designed an optimal control strategy with linear state feedback according to the linear regulator theory. For a tethered system in orbital plane, Williams [5] proposed a receding-horizon controller, which exhibits relatively higher computational efficiency. Steindl et al. [6] designed an optimal controller to achieve a force controlled retrieval of the tethered subsatellite system. Jin and Hu [7] proposed a strategy based on the combination of quasi linearization and truncated Chebyshev series to solve the constrained nonlinear optimal control problem of the tethered subsatellite system. Recently, Wen et al. [8] designed an optimal feedback control law for the deployment process of a tethered subsatellite based on real-time trajectory generation and online grid adaptation. In all of these studies, the tether was modeled as an inextensible cable for controller design. However, the effect of longitudinal tether vibrations can cause errors in the position and velocity of the tether tip. To improve the control performance, the elasticity of the tether was considered in some recent work, but limited to the in-plane motion. For instance, Williams and Trivailo [9] and Williams [10] made a comparison of various cost functions for the optimal control of a tethered satellite system and used an elastic tether system for rendezvousing and capturing a payload.

This paper is devoted to finding an optimal trajectory that guides the subsatellite from an initial position far from the spaceship into a final position close to the spaceship. In this study, in addition to the usually addressed pitch (in-plane) motion, the roll (out-of-plane) motion was also taken into account. The previous studies in [7,8] are extended here to a more realistic model involving a longitudinally flexible tether. Furthermore, this work introduces two new developments in the field of infinite-horizon nonlinear optimal control. The first of these is the application of the existing direct pseudospectral algorithm, developed by Fahroo and Ross [11], to discretize the optimal control problem and to numerically solve the resulting large-scale optimization problem via an nonlinear programming (NLP) solver. The second innovation is an indirect solution method based on successive linear approximations obtained via the method of quasi linearization, similar to the method presented in [5], except for the way that the infinite horizon is handled. That is, a domain-transformation technique is exploited in this work instead of the usually adopted receding-horizon framework, which may impose other challenges such as stability and selection of the fixed horizon

Received 3 July 2007; revision received 5 November 2007; accepted for publication 8 November 2007.

*Ph.D. Candidate, Ministry of Education Key Laboratory of Structure Mechanics and Control for Aircraft; wenhao@nuaa.edu.cn.

†Professor, Ministry of Education Key Laboratory of Structure Mechanics and Control for Aircraft; jindp@nuaa.edu.cn.

‡Professor, Ministry of Education Key Laboratory of Structure Mechanics and Control for Aircraft; hhyae@nuaa.edu.cn.

[12]. Another important difference between the proposed method and the method in [5] is the way that the initial condition is incorporated. This work relaxes the differential constraint at the last node instead of at the first node. The reason for this change is to improve the precision of the control signal closed to the initial node. The proposed strategies were coded into a reusable general optimal control package based on an object-oriented framework in C++ language and numerically demonstrated through case studies.

II. Problem Formulation

As shown in Fig. 1, the system under consideration consists of a spaceship of mass M and a subsatellite of mass m connected by a straight massless tether of variable length $l(t)$ and longitudinal stiffness EA. The longitudinal elongation of the tether is characterized by its strain ε (assumed uniform along the tether). In most studies (for instance, in [7]), the assumption $m \ll M$ is made such that the orbit center of the system can be assumed to coincide with the mass center of the spaceship, which moves on a circular Keplerian orbit of height r_0.

From a practical point of view, the initial roll angle and its rate are not strictly of zero values, due to control errors in the early deployment phase or external disturbances. Therefore, out-of-plane motion is taken into account in this work. The spaceship and subsatellite are modeled by a point-mass approximation, and the attitude of the tether is given by the in-plane pitch angle θ and the out-of-plane roll angle φ. This formulation enjoys the advantage of low computational effort required for optimization and controller design. One difficulty is how to apply the control action to the system. A hybrid strategy using the tension control augmented by the out-of-plane thruster is adopted in this study, because tension control laws are more effective when used in conjunction with out-of-plane thrusting [2].

A. Mathematical Model

By a straightforward application of Lagrange's equations, as detailed in [13], with the generalized coordinate vector

$$\mathbf{q} = \{\theta, \varphi, \xi, \varepsilon\}^T \in \mathbb{R}^{n_q}$$

the dynamic equation of the subsatellite in dimensionless form reads

$$\begin{aligned}
&(1+\varepsilon)\xi\ddot{\theta} + 2(\dot{\theta}-1)(\xi\dot{\varepsilon} + (1+\varepsilon)(\dot{\xi} - \xi\dot{\varphi}\tan\varphi)) \\
&\quad + 3(1+\varepsilon)\xi\sin\theta\cos\theta = 0 \\
&(1+\varepsilon)\xi\ddot{\varphi} + 2\dot{\varphi}(\xi\dot{\varepsilon} + (1+\varepsilon)\dot{\xi}) \\
&\quad + (1+\varepsilon)\xi(3\cos^2\theta + (\dot{\theta}-1)^2)\sin\varphi\cos\varphi = F/(m\Omega^2 l_c) \\
&(1+\varepsilon)\ddot{\xi} + 2\dot{\xi}\,\dot{\varepsilon} + \xi\ddot{\varepsilon} - (1+\varepsilon)\xi((\dot{\theta}-1)^2\cos^2\varphi \\
&\quad + \dot{\varphi}^2 + 3\cos^2\theta\cos^2\varphi - 1) = -T/(m\Omega^2 l_c)
\end{aligned} \tag{1}$$

where $\xi = \tilde{l}(t)/l_c$ is the dimensionless unstrained tether length, with $\tilde{l}$ and l_c being the current and commanded tether lengths (unstrained),

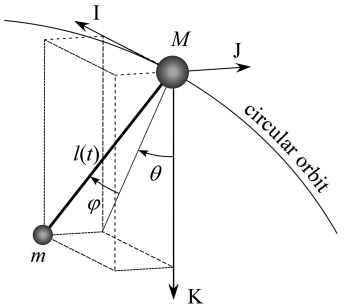

Fig. 1 Schematic view of a tethered subsatellite system on a circular orbit at angular rate Ω. The I coordinate points in the flight direction of the spaceship, the J coordinate is perpendicular to the orbit plane, and the K coordinate points to the center of the Earth.

respectively, and the dot represents the derivative with respect to the dimensionless time t through the use of a scaling factor Ω. In Eq. (1), $T = EA\varepsilon$ is the tensional force along the tether and F is the out-of-plane thrust. The orbital angular velocity reads $\Omega = \sqrt{\mu/r_0^3}$, where

$$\mu = 3.986005 \times 10^{14}\ \mathrm{m}^3/\mathrm{s}^2$$

is the gravitational parameter of the Earth.

The control inputs are assumed to be strain acceleration $u_1 = \ddot{\varepsilon}$ and dimensionless out-of-plane thrust $u_2 = F/(m\Omega^2 l_c)$. Through a straightforward linear transformation, Eq. (1) can be recast into the following state-space form:

$$\begin{aligned}
&\dot{x}_1 = x_5, \qquad \dot{x}_2 = x_6, \qquad \dot{x}_3 = x_7, \qquad \dot{x}_4 = x_8, \\
&\dot{x}_5 = -(2x_5 - 2)\left(\frac{x_7}{x_3} - x_6\tan(x_2) + \frac{x_8}{1+x_4}\right) - 3/2\sin(2x_1), \\
&\dot{x}_6 = -2x_6\left(\frac{x_7}{x_3} + \frac{x_8}{1+x_4}\right) - 1/2\sin(2x_2)((x_5-1)^2 \\
&\quad + 3(\cos(x_1))^2) + \frac{u_2}{x_3(1+x_4)}, \\
&\dot{x}_7 = -\frac{2x_7x_8 + x_3u_1}{1+x_4} + x_3((x_5-1)^2(\cos(x_2))^2 + x_6^2 \\
&\quad + 3(\cos(x_1))^2(\cos(x_2))^2 - 1) - \frac{EAx_4}{m\Omega^2 l_c(1+x_4)}, \\
&\dot{x}_g = u_1
\end{aligned} \tag{2}$$

where $x_i (i = 1, 2, \ldots, 8)$ denotes the entries in the state vector $\mathbf{x} = \{\theta, \varphi, \xi, \varepsilon, \dot{\theta}, \dot{\varphi}, \dot{\xi}, \dot{\varepsilon}\}^T$.

B. Statement of Optimal Control Problem

This work is devoted to finding an optimal trajectory that guides the subsatellite from an initial position far from the spaceship into a final position close to the spaceship. In terms of infinite-horizon optimal control, the problem under consideration is to look for the state-control pair

$$[0 \quad \infty) \ni t \mapsto \{\mathbf{x} \in \mathbb{R}^{n_x}, \mathbf{u} \in \mathbb{R}^{n_u}\}$$

to minimize the cost functional

$$J[\mathbf{x}(\cdot), \mathbf{u}(\cdot)] = \int_0^\infty F(\mathbf{x}(t), \mathbf{u}(t), t)\,\mathrm{d}t \tag{3}$$

which is subject to dynamic constraints

$$\dot{\mathbf{x}} = \mathbf{f}(\mathbf{x}(t), \mathbf{u}(t)) \tag{4}$$

and endpoint constraints

$$\mathbf{x}(0) = \mathbf{x}_0 \tag{5}$$

where $\mathbf{x}_0$ is a known vector of initial conditions and both of the functions

$$F: \ \mathbb{R}^{n_x} \times \mathbb{R}^{n_u} \times \mathbb{R} \mapsto \mathbb{R}, \qquad \mathbf{f}: \ \mathbb{R}^{n_x} \times \mathbb{R}^{n_u} \mapsto \mathbb{R}^{n_x} \tag{6}$$

are assumed to be continuously differentiable with respect to their arguments. The differential constraints [namely, Eq. (2)] were generalized to the form of Eq. (4), and the initial conditions of the retrieval are represented by Eq. (5). To simplify the analysis, the performance index is assumed to be of the quadratic form usually encountered in practice: namely,

$$\begin{aligned}
F(\mathbf{x}(t), \mathbf{u}(t), t) = \tfrac{1}{2}[&(\mathbf{x}(t) - \mathbf{x}_d(t))^T\mathbf{Q}(\mathbf{x}(t) - \mathbf{x}_d(t)) \\
&+ (\mathbf{u}(t) - \mathbf{u}_d(t))^T\mathbf{R}(\mathbf{u}(t) - \mathbf{u}_d(t))]
\end{aligned} \tag{7}$$

where $\mathbf{x}_d \in \mathbb{R}^{n_x}$ and $\mathbf{u}_d \in \mathbb{R}^{n_u}$ are, respectively, the desired states and control inputs during the retrieval, $\mathbf{Q}$ is a positive semidefinite matrix, and $\mathbf{R}$ is a positive definite matrix. Note that the nonlinearity

in system dynamics was taken into consideration in Eq. (4). There is an important distinction between the usual linear quadratic control design and the problem posed by Eqs. (3–5).

III. Pseudospectral Methods

With the advent of digital computer and efficient computational algorithms, many techniques have been available for numerically solving nonlinear optimal control problems on a finite horizon. Among them, a class of approaches is often referred to as the direct approaches, which discretize the optimal control problem to a parameter optimization problem and then solve the resulting NLP problem. The indirect approaches, in contrast, entail forming the optimization conditions directly and then solving the resulting equations with associated boundary conditions (e.g., the multiple shooting methods presented in [6]). However, all the methods shall be applied subject to modifications when the infinite-horizon optimal control is considered. The central computational problem is the treatment of the infinite horizon. The standard approach to this problem has been to approximate the infinite-horizon problem by a sequence of suboptimal receding finite-horizon problems, which may impose other challenges such as stability and selection of the fixed horizon. To circumvent these issues, a domain-transformation technique is exploited in this paper based on the recent work by Fahroo and Ross [11]. In this way, the infinite horizon is mapped to a finite computational domain so that the optimal control problem can be solved via the aforementioned direct or indirect approaches.

With the aid of the domain transformation, two pseudospectral algorithms are explored to solve the optimal control problem stated in the previous section. The first of these is the application of the existing direct algorithm, developed by Fahroo and Ross [11], which involves direct transcription and nonlinear programming. The second one is a new indirect solution method based on successive linear approximations obtained via the method of quasi linearization. Both of the strategies share the same discretization algorithm in the background (i.e., the Legendre pseudospectral method, which features a high convergence rate and ease of implementation [11,12]). The basic idea of this algorithm is to use the polynomial approximations for the state and control variables at the Legendre–Gauss–Radau (LGR) points first and then to approximate the state derivatives in terms of the state variables at the LGR points via a differentiation matrix. All path constraints [for example, Eq. (4)] are only imposed at LGR points.

A. Domain Transformation

Let $L_N(\tau)$ be the Legendre polynomial of N deg. The LGR points τ_n are given by the $N+1$ roots of $L_N(\tau)+L_{N+1}(\tau)$ for $0 \le n \le N$ and include a fixed abscissa at $\tau_0 = -1$. Because the LGR points lie in the interval $[-1 \quad 1)$, the infinite-horizon optimal control problem is reformulated via a domain transformation [12] so that the LGR nodes can be used for interpolation polynomials. The original semi-infinite time interval $t \in [\mathbf{0} \quad \infty)$ is mapped to the finite computational domain $\tau \in [-1 \quad 1)$ through the following rational transformation:

$$t = \frac{1+\tau}{1-\tau} \leftrightarrow \tau = \frac{t-1}{t+1} \tag{8}$$

The transformed optimal control problem is now formulated as follows:

Find the state-control pair

$$[-1 \quad 1) \ni \tau \mapsto \{\mathbf{x} \in \mathbb{R}^{n_x}, \mathbf{u} \in \mathbb{R}^{n_u}\}$$

to minimize the cost functional

$$J[\mathbf{x}(\cdot), \mathbf{u}(\cdot)] = \int_{-1}^{1} F(\mathbf{x}(\tau), \mathbf{u}(\tau), \tau) r(\tau)\, \mathrm{d}\tau \tag{9}$$

which is subject to dynamic constraints

$$\mathbf{x}' = r(\tau)\mathbf{f}(\mathbf{x}(\tau), \mathbf{u}(\tau)) \tag{10}$$

and initial conditions

$$\mathbf{x}(-1) = \mathbf{x}_0 \tag{11}$$

In the preceding formulations, all functional evaluations at $\tau = 1$ or $t = \infty$ are taken in the sense of a limit, the prime represents the derivative with respect to time τ, and $r(\tau)$ is given by

$$r(\tau) = \frac{\mathrm{d}t}{\mathrm{d}\tau} = \frac{2}{(1-\tau)^2} \tag{12}$$

B. Direct Legendre Pseudospectral Method

As presented in [11], the states and controls are approximated by the Nth-deg polynomials in the form

$$\begin{aligned} x_i(\tau) &\doteq x_i^N(\tau) = \sum_{j=0}^{N} x_i(\tau_j)\phi_j(\tau), \qquad i = 1, 2, \cdots, n_x \\ u_i(\tau) &\doteq u_i^N(\tau) = \sum_{j=0}^{N} u_i(\tau_j)\phi_j(\tau), \qquad i = 1, 2, \cdots, n_u \end{aligned} \tag{13}$$

where $x_i(\tau)$ and $u_i(\tau)$ are the ith entry in the vector functions $\mathbf{x}(\tau)$ and $\mathbf{u}(\tau)$, and the basis functions $\phi_j(\tau)$ are the Lagrange interpolation polynomials that satisfy

$$\phi_j(\tau_i) = \begin{cases} 1 & \text{if } i = j \\ 0 & \text{if } i \ne j \end{cases} \tag{14}$$

The dynamic equation (10) is stratified at the LGR points $\tau_i (i = 0, 1, \ldots, N)$ in the following form:

$$\mathbf{f}(\mathbf{x}(\tau_i), \mathbf{u}(\tau_i)) - \frac{1}{r(\tau_i)} \sum_{j=0}^{N} D_{ij}\mathbf{x}(\tau_j) = 0 \tag{15}$$

where $D_{ij} = \phi_j'(\tau_i)$ are the entries in the $(N+1) \times (N+1)$ differentiation matrix $\mathbf{D}$. Furthermore, approximating the Lagrange cost function in Eq. (9) by Gauss–Radau quadrature rules yields

$$J \doteq \sum_{k=0}^{N} w_k r(\tau_k) F(\mathbf{x}(\tau_k), \mathbf{u}(\tau_k), \tau_k) \tag{16}$$

where w_k are the LGR integration weights given by

$$w_0 = \frac{2}{(N+1)^2}, \qquad w_j = \frac{1-\tau_j}{(N+1)^2[L_N(\tau_j)]^2}, \qquad 1 \le j \le N \tag{17}$$

At this point, the trajectory optimization problem described by Eqs. (3–5) has been transformed into a standard NLP problem with the cost function in Eq. (16), the constraints in Eqs. (11) and (15), and $(N+1)(n_x+n_u)$ parameters, which consist of $\mathbf{x}(\tau_k)$ and $\mathbf{u}(\tau_k)$ at LGR points for $k = 0, 1, \ldots, N$. Many off-the-shelf NLP solvers are available for solving such a problem routinely. This work adopts an NLP-solving engine named IPOPT, which implements an interior point line-search filter method and has found many successful applications [14].

C. Method of Quasi Linearization

To solve the nonlinear optimal control problem, the first step of the proposed algorithm is to apply the second method of quasi linearization [5], in which the system equations (4) are expanded to first order and the performance index (3) is expanded up to the second order around a reference trajectory. Then the original problem described by Eqs. (3–5) is reduced to the following sequence of linear optimal control problems by using the same domain transformation:

$$\min(J^{(k+1)}) = \min\left(\int_{-1}^{1} r(\tau) F(\mathbf{x}^{(k+1)}(\tau), \mathbf{u}^{(k+1)}(\tau), \tau)\, \mathrm{d}\tau \right) \tag{18}$$

subject to

$$\mathbf{x}'^{(k+1)}(\tau) = r(\tau)(\mathbf{A}^{(k)}(\tau)\mathbf{x}^{(k+1)}(\tau) + \mathbf{B}^{(k)}(\tau)\mathbf{u}^{(k+1)}(\tau) + \mathbf{h}^{(k)}(\tau)),$$
$$\mathbf{x}^{(k+1)}(-1) = \mathbf{x}_0 \tag{19}$$

where

$$F(\mathbf{x}^{(k+1)}, \mathbf{u}^{(k+1)}, \tau) = \tfrac{1}{2}[(\mathbf{x}^{(k+1)} - \mathbf{x}_d)^T\mathbf{Q}(\mathbf{x}^{(k+1)} - \mathbf{x}_d) + (\mathbf{u}^{(k+1)} - \mathbf{u}_d)^T\mathbf{R}(\mathbf{u}^{(k+1)} - \mathbf{u}_d)] \tag{20}$$

$$\mathbf{h}^{(k)} = \mathbf{f}(\mathbf{x}^{(k)}, \mathbf{u}^{(k)}) - \mathbf{A}^{(k)}\mathbf{x}^{(k)} - \mathbf{B}^{(k)}\mathbf{u}^{(k)} \tag{21}$$

$$\begin{cases} \mathbf{A}^{(k)} = \partial\mathbf{f}(\mathbf{x}, \mathbf{u})/\partial\mathbf{x}|_{\mathbf{x}^{(k)}, \mathbf{u}^{(k)}} \in \mathbb{R}^{n\times n} \\ \mathbf{B}^{(k)} = \partial\mathbf{f}(\mathbf{x}, \mathbf{u})/\partial\mathbf{u}|_{\mathbf{x}^{(k)}, \mathbf{u}^{(k)}} \in \mathbb{R}^{n\times n} \end{cases} \tag{22}$$

$\mathbf{x}^{(k+1)}(\tau)$ and $\mathbf{u}^{(k+1)}(\tau)$ are the state and control vectors for the current $(k+1)$th quasi-linearization iteration, and $\mathbf{x}^{(k)}(\tau)$ and $\mathbf{u}^{(k)}(\tau)$ are the state and control vectors from the previous kth iteration and are taken as the reference trajectories for the current computation.

At the $(k+1)$th iteration, introduce the Hamiltonian function $H^{(k+1)}$ defined by

$$H^{(k+1)} = rF + (\boldsymbol{\lambda}^{(k+1)})^T[r(\mathbf{A}^{(k)}\mathbf{x}^{(k+1)} + \mathbf{B}^{(k)}\mathbf{u}^{(k+1)} + \mathbf{h}^{(k)})] \tag{23}$$

where $\boldsymbol{\lambda}^{(k+1)} \in \mathbb{R}^n$ is the costate vector for the current iteration and superscript T represents a transpose of the vector or matrix. On invoking the principle of optimality, it can be shown that the optimal solution is characterized by the following sets of differential equations:

$$\frac{1}{r(\tau)}\begin{bmatrix}\mathbf{x}'^{(k+1)} \\ \boldsymbol{\lambda}'^{(k+1)}\end{bmatrix} = \begin{bmatrix}\mathbf{A}^{(k)} & -\mathbf{B}^{(k)}\mathbf{R}^{-1}(\mathbf{B}^{(k)})^T \\ -\mathbf{Q} & -(\mathbf{A}^{(k)})^T\end{bmatrix}\begin{bmatrix}\mathbf{x}^{(k+1)} \\ \boldsymbol{\lambda}^{(k+1)}\end{bmatrix} + \begin{bmatrix}\mathbf{B}^{(k)}\mathbf{u}_d + \mathbf{h}^{(k)} \\ \mathbf{Q}\mathbf{x}_d\end{bmatrix} \tag{24}$$

subject to the boundary conditions

$$\mathbf{x}^{(k+1)}(-1) = \mathbf{x}_0, \qquad \boldsymbol{\lambda}^{(k+1)}(1) = 0 \tag{25}$$

Through a similar discretization process as in the previous subsection, the continuous-vector equation (24) can be converted to a set of linear algebraic equation by collocating at the LGR nodes as follows:

$$\frac{1}{r}\sum_{j=0}^{N} D_{ij}\mathbf{x}^{(k+1)}(\tau_j) - \mathbf{A}^{(k)}\mathbf{x}^{(k+1)}(\tau_i) + \mathbf{B}^{(k)}\mathbf{R}^{-1}(\mathbf{B}^{(k)})^T\boldsymbol{\lambda}^{(k+1)}(\tau_i) = \mathbf{B}^{(k)}\mathbf{u}_d + \mathbf{h}^{(k)} \tag{26a}$$

$$\frac{1}{r}\sum_{j=0}^{N} D_{ij}\boldsymbol{\lambda}^{(k+1)}(\tau_j) + \mathbf{Q}\mathbf{x}^{(k+1)}(\tau_i) + (\mathbf{A}^{(k)})^T\boldsymbol{\lambda}^{(k+1)}(\tau_i) = \mathbf{Q}\mathbf{x}_d \tag{26b}$$

where $\mathbf{A}^{(k)}$, $\mathbf{B}^{(k)}$, $\mathbf{h}^{(k)}$, $\mathbf{x}_d$, $\mathbf{u}_d$, and r are evaluated at τ_i $(i = 0, 1, \ldots, N)$. At this point, the optimal control problem described by Eqs. (18–22) has been transformed into a set of linear algebraic equations. The boundary conditions (25) are incorporated by replacing the last n equations in Eq. (26a) with

$$\mathbf{x}^{(k+1)}(\tau_0) = \mathbf{x}_0 \tag{27a}$$

and replacing the last n equations in Eq. (26b) with

$$\boldsymbol{\lambda}^{(k+1)}(\tau_N) = 0 \tag{27b}$$

A slight but important difference between the proposed method and the method in [5] is the way that the initial condition is incorporated. The proposed method relaxes the differential constraint at the last node instead of at the first node. In other words, the state equation at τ_N, rather than at τ_0, is replaced with the initial conditions (27a), which favors closed-loop control because only the control signal closed to the initial node is implemented.

It is worth noticing that

$$\boldsymbol{\lambda}^{(k+1)} = 0|_{\tau=1}$$

is approximately satisfied at τ_N in Eq. (27b) for numeric implementation. That is, evaluation at the right-hand point (which for the mapped domain corresponds to $t = \infty$) is at $\tau_N = 1 - \varepsilon$, where the size of ε depends inversely on N (namely, $\varepsilon \to 0$ as $N \to \infty$). The discrete values of states and costates at LGR points can be obtained by simultaneously solving $2(N+1)n_x$ linear algebraic equations, including Eqs. (26a) and (26b) for $i = 0, 1, \ldots, N-1$ and Eqs. (27a) and (27b), with $2(N+1)n_x$ variables [namely, the components of $\mathbf{x}^{(k+1)}$ and $\boldsymbol{\lambda}^{(k+1)}$ at τ_i for $i = 0, 1, \ldots, N$]. As soon as $\mathbf{x}^{(k+1)}$ and $\boldsymbol{\lambda}^{(k+1)}$ are obtained, the control input $\mathbf{u}^{(k+1)}$ can be easily determined and Eqs. (26a) and (26b) will be updated in terms of the new solution [5]. At each iteration, the asymmetric sparse linear systems are solved by a free numeric library named UMFPACK, based on direct sparse lower/upper factorization [15].

IV. Case Studies

The presented algorithms are coded into a reusable general optimal control package based on an object-oriented framework in C++ language, which enjoys a real-time advantage over the usual MATLAB scripting method. The computation loads of the direct algorithm are reduced with the aid of a symbolic preprocessor to obtain the analytical Jacobians and Hessians. In addition, for both algorithms, the computation and memory efficiency are improved by putting the sparse structures of involved matrices into full use.

The performance of the proposed controllers is demonstrated through three case studies on a representative system which, as shown in Fig. 1, is assumed to move on a circular orbit at a distance of $r_0 = 6771$ km from the center of the Earth (namely, at an altitude of approximately 400 km). The angular velocity Ω is computed to be about 1.133×10^{-3} rad/s. The subsatellite mass m is assumed to be 100 kg, the mass M of the spaceship is 1×10^5 kg, the longitudinal stiffness is $EA = 1 \times 10^5$ N, and the commanded length (unstrained) $l_c = 10$ km. The required weighting matrices $\mathbf{Q}$ and $\mathbf{R}$ for the controller design are chosen to be

$$\begin{aligned}\mathbf{Q} &= 2 \times \mathrm{diag}(\{10^3, 10^3, 10^3, \alpha^2, 10^3, 10^3, 10^3, \alpha^2\}), \\ \mathbf{R} &= 2 \times \mathrm{diag}(\{10\alpha^2, 10^3\})\end{aligned} \tag{28}$$

where diag represents the diagonal matrix with diagonal elements taken from a vector, and the factor

$$\alpha = \frac{EA}{m\Omega^2 l_c} \tag{29}$$

is used to scale the strain, strain rate, and strain acceleration of the tether, which are much smaller in magnitude than the other variables.

In this work, the retrieval maneuver is considered to begin with the initial states

$$\mathbf{x}_0 = \{\theta_0, \varphi_0, \xi_0, \varepsilon_0, \dot{\theta}_0, \dot{\varphi}_0, \dot{\xi}_0, \dot{\varepsilon}_0\}$$

and to be stabilized around the desired state trajectory $\mathbf{x}_d$, which is simply taken to be a constant vector

$$\{\theta_d, \varphi_d, \xi_d, \varepsilon_d, \dot{\theta}_d, \dot{\varphi}_d, \dot{\xi}_d, \dot{\varepsilon}_d\}$$

(i.e., the desired states at the end of retrieval). Here, the initial and desired final values are denoted by the subscripts 0 and d, respectively. The first case study is subject to a nominal initial value

$$\mathbf{x}_0|_{\text{case1}} = \{0, 0, 1, \varepsilon_0|_{\text{case1}}, 0, 0, 0, 0\}$$

whereas a medium degree of initial angle perturbations is taken into consideration in the other two cases: namely,

$$\mathbf{x}_0|_{\text{case2}} = \{0.1, 0, 1, \varepsilon_0|_{\text{case2}}, 0, 0, 0, 0\}$$

and

$$\mathbf{x}_0|_{\text{case3}} = \{0.1, 0.05, 1, \varepsilon_0|_{\text{case3}}, 0, 0, 0, 0\}$$

where all the angles are given in radians. The retrieval motions of all cases are supposed to be stabilized around the same

$$\mathbf{x}_d = \{0, 0, 0.1, \varepsilon_d, 0, 0, 0, 0\}$$

which corresponds to a radial equilibrium configuration near the spaceship. It is worth noticing that the tether strain has not been listed here in numeric form. In each of the cases, the initial and desired final values of tether strain are assumed to be a set of nominal values, which are given by additionally substituting $\ddot{\varepsilon} = 0$ and $\ddot{\xi} = 0$ into the last row of Eq. (1).

For all three case studies, the guesses for control inputs (namely, strain acceleration $u_1 = \ddot{\varepsilon}$ and dimensionless out-of-plane thrust u_2) are simply chosen to be zero over the entire time domain, whereas all the guesses for states are arbitrarily set to the initial values of $\mathbf{x}_0$. As the ending criterion, the pseudolinearization iteration is designed to be terminated if and only if

$$|\alpha(u_1^{(k+1)} - u_1^{(k)})| \le 10^{-6}$$

and

$$|u_2^{(k+1)} - u_2^{(k)}| \le 10^{-6}$$

are simultaneously satisfied at all LGR points. Although a substantially smaller number of nodes is sufficient for satisfying the precision needs of real-time optimal control, all the problems are discretized with 70 LGR nodes to guarantee an accurate comparison of the direct and indirect (quasi-linear) algorithms. The optimal solutions are obtained on a 1.73-GHz Pentium M laptop within 15 s by using both algorithms, the comparison of which reveals that two solutions agree with each other very well, except at the final LGR node. The optimal control profiles of a representative case (namely, case 3) are selected to demonstrate the agreement in detail. In Fig. 2, with respect to the dimensionless time t, the optimal control profiles obtained via the two groups of algorithms are illustrated by solid lines (direct solution) and circles (indirect solution), respectively. It can be seen that the optimal profiles for strain acceleration u_1 and dimensionless thrust u_2 are almost the same under the two methods. Additionally, it is worth noticing that the computational costs of the direct method are ranging between 6 and 15 s in different cases, whereas time costs of the indirect approach are relatively stable at about 11 s for all the three cases. This is because the controls and system responses obtained by the direct algorithm match the indirect solutions so well that they are indistinguishable in the figures. Hence, only the latter is shown in the following figures.

In Fig. 3, the time histories of optimal control profiles are presented with respect to the dimensionless time t. The top figure gives the optimal profiles of strain acceleration u_1, which exhibits some oscillatory behavior in the beginning. The oscillation of u_1 is damped quickly and the control trajectories converge fast to zero, as desired. The time histories of strain acceleration in case 2 are almost the same as in case 3 and only slightly different from that in case 1 at the early stage of retrieval. However, as seen from the bottom figure, the thruster is inactive in the first two cases, the thrust profiles of which are significantly different from that in case 3. During the retrieval, the dimensionless thrusts in cases 1 and 2 remain permanently zero, whereas the optimal thrust profiles in case 2 begin with a short-term oscillation and then converge quickly to zero. It can be seen that for the presented cases, the initial out-of-plane angle perturbations are mainly counteracted by the thrust, whereas in-plane angle disturbances are influenced by tether tension.

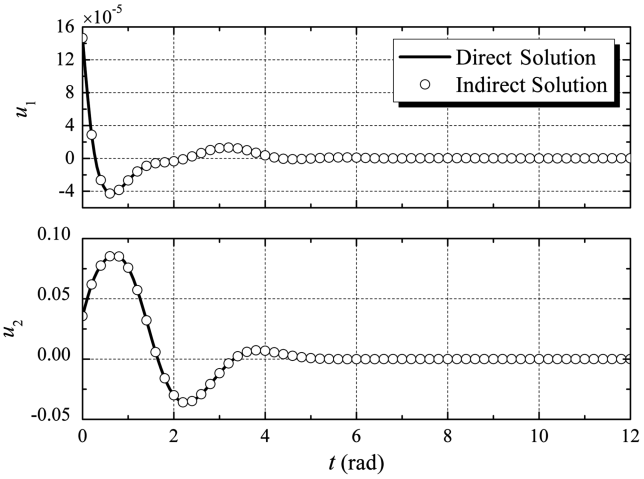

Fig. 2 Comparison of the optimal profiles for strain acceleration u_1 and dimensionless thrust u_2 using direct and indirect solutions.

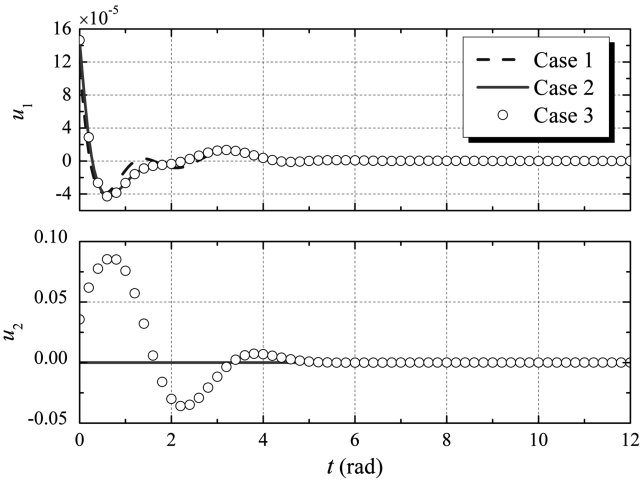

Fig. 3 Comparison of the optimal profiles for strain acceleration u_1 and dimensionless thrust u_2 in the three case studies.

To gain an insight into the retrieval dynamics, Fig. 4 shows the time histories of dimensionless system variables under the optimal control scheme for three cases in which the system is subject to different initial values. As seen from the first to the fourth rows of Fig. 4, the pitch, roll, length (unstrained), and strain dynamics were almost brought to the desired values at $t = 12$. At this moment, under the proposed nonlinear optimal control scheme, the system states get so close to the desired value $\mathbf{x}_d$ that the much simpler linear control can be applied. Of course, such a control is effective only in the case of small-amplitude oscillations. Additionally, as shown in Figs. 4c and 4d, the roll motion cannot be excited in the first two cases, whereas the time histories of roll motion in case 3 exhibit some oscillatory behavior in the beginning and then converge quickly to zero, as desired. As the other plots indicate, the optimal profiles for θ, $\dot{\theta}$, ξ, $\dot{\xi}$, ε, and $\dot{\varepsilon}$ in case 2 are almost the same as in case 3 and are only slightly different from those in case 1 in the beginning parts of retrieval maneuver, each with different initial pitch angles.

From a practical point of view, there are some issues that deserve further investigation. For example, it is a common practice for real-time optimal control to maximize computational efficiency by using as few as possible discretization nodes. However, to meet the precision requirement of a practical mission, a lower bound must be enforced for the number of nodes. In regard to the precision of online control, the initial inputs should receive special attention, because only the control signal closed to τ_0 needs to be implemented. In Fig. 5, a representative case (namely, case 3) is selected to compare $\mathbf{u}(\tau_0)$, solved by using different algorithms and different number of

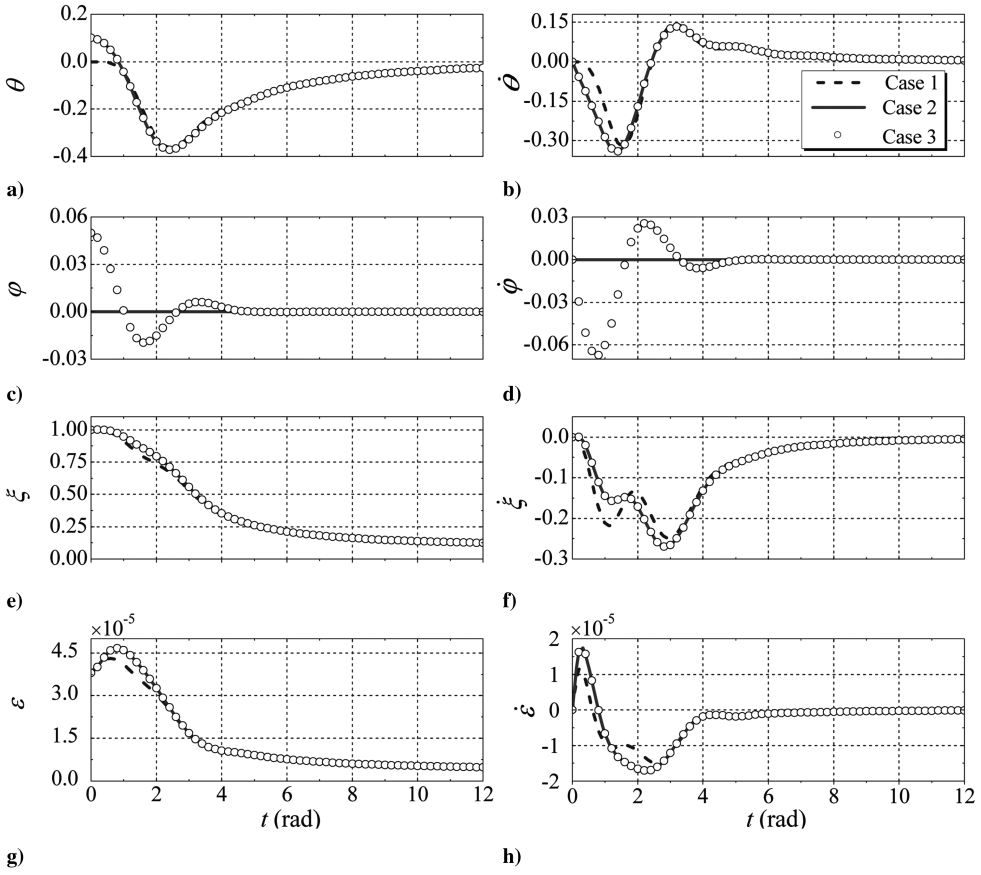

Fig. 4 Comparison of the optimal profiles for state variables θ, $\dot{\theta}$, φ, $\dot{\varphi}$, ξ, $\dot{\xi}$, ε, and $\dot{\varepsilon}$ in the three case studies.

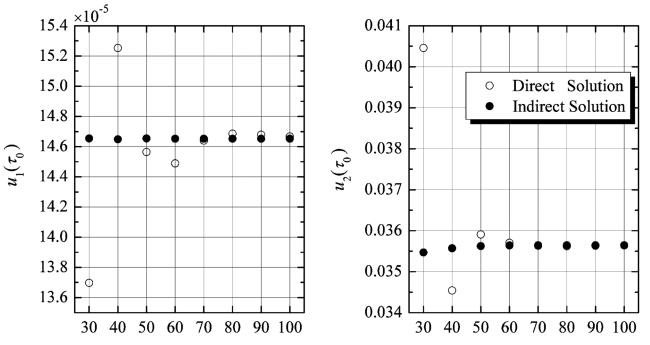

Fig. 5 Comparison of the initial control inputs $\mathbf{u}(\tau_0)$ from direct and indirect solutions by using different number of LGR nodes.

nodes. As shown in the figure, the solutions obtained by using both algorithms agree well with each other as long as the number of nodes is greater than 60. An analytic solution to this problem is unavailable. Hence, the solution with 100 nodes is taken as a reference for further comparison, which reveals that the direct solutions are more sensitive to the decrease of the number of nodes. It is also shown that the indirect method is extremely competitive in terms of precision as the number of nodes becomes less than 50.

Another point of practical interest is to implement the proposed control strategies for the purely tension-controlled problem, which requires less effort with the equipment. It was demonstrated that full three-dimensional motions can be extinguished via the tension control augmented by an out-of-plane thruster. However, it is not the same case when acting on the motion of the system by changing only the tensional force. The point will be made clear by linearizing Eq. (2) about the desired value $\mathbf{x}_d$ and setting u_2 to be zero. In regard to the roll (out-of-plane) motion, the locally linearized equation reads

$$\dot{x}_6 + 4x_2 = 0 \Leftrightarrow \ddot{\varphi} + 4\varphi = 0 \tag{30}$$

which indicates that the roll motion is almost independent of the other two degrees of freedom and oscillates harmonically with period $T_\varphi \doteq \pi$, as the system state becomes sufficiently close to $\mathbf{x}_d$. The idea of online trajectory generation is incorporated into the following solution process, because long-term oscillations cannot be accurately described by open-loop trajectories, even with a significant number of (polynomial) basis functions. The online controller is implemented by using a rapid recomputation of open-loop optimal control online with 50 nodes and updating the control command at a dimensionless sampling time of 0.1 rad. During the online simulation, the initial condition of the $(s+1)$th computation (namely, the state at the current sampling time) is determined by propagating the system dynamics from the initial states of the sth run. Here, s represents the sequence number of each online computation and $s = 0$ corresponds to a startup offline run. The initial guesses for the $(s+1)$th computation are simply taken from the results of the sth step without interpolation. It is observed that the direct method becomes especially slow and unstable when the purely tension-controlled problem is regarded. Hence, only the indirect method is used as the underlying trajectory-generation method for each online step. Some issues concerning closed-loop control, such as computational delay and state prediction, are not dealt with here because this study focuses on the performance of the methods used for trajectory generation.

Taking case 3, for example, Fig. 6 demonstrates the time histories of dimensionless state variables θ, φ, ξ, and ε under the proposed infinite-horizon control (IHC). Here, $\mathbf{x}_0|_{\text{case1}}$ is taken as the initial value for the startup offline computation. For comparison, the figure also includes the solutions obtained by applying the receding-horizon control (RHC) scheme in [5], which is designed to optimize the following performance index:

$$J = (\mathbf{x}(t_f) - \mathbf{x}_d)^T \Theta_f (\mathbf{x}(t_f) - \mathbf{x}_d) + \int_0^{t_f} F(\mathbf{x}(t), \mathbf{u}(t), t)\, \mathrm{d}t \tag{31}$$

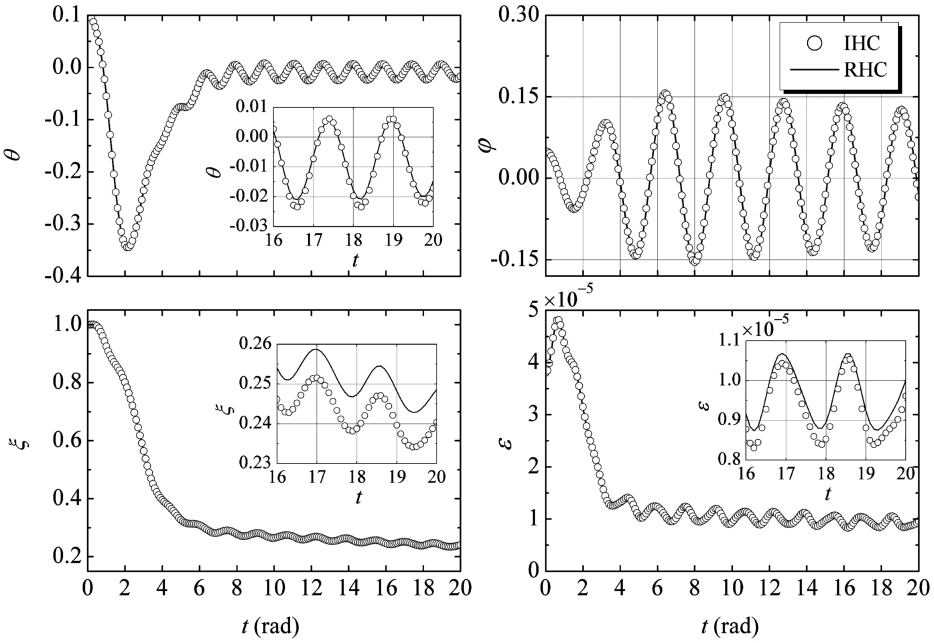

Fig. 6 Comparison of the trajectories for state variables θ, φ, ξ, and ε solved by using IHC and RHC schemes (full-range and partial enlargement views).

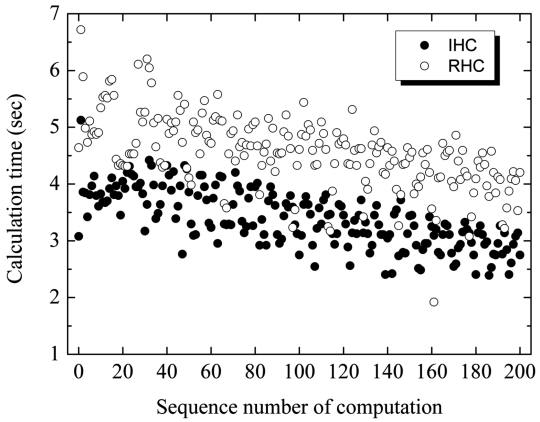

Fig. 7 Comparison of the time cost of each online computation by using IHC and RHC schemes.

where the horizon length t_f is chosen to be 6 rad and

$$\Theta_f = 1 \times 10^3 \ \mathrm{diag}(\{1, 1, 1, \alpha^2, 1, 1, 1, \alpha^2\})$$

The initial guesses for the RHC controller are determined in the same way as in the IHC scheme, to facilitate a fair comparison. Figure 6 gives two solutions from IHC, and RHC schemes are only slightly different from each other. As shown in Fig. 6, the tension control laws are less effective without the aid of out-of-plane thrusting, but are still capable of stabilizing the system motions that become slowly damped oscillations when the subsatellite is close to the spaceship. Figure 6 also shows that the oscillation period of roll angle is almost the same as described in Eq. (30). For each online computation, a comparison of computational time costs (in seconds) by using IHC and RHC schemes is given in Fig. 7, in which the interval between each step is 0.1 rad and the startup offline run is denoted by a sequence number equal to zero. As shown in Fig. 7, the proposed IHC scheme enjoys a considerable computational advantage over the RHC method.

V. Conclusions

The paper presents optimal schemes for controlling the three-dimensional retrieval process of a tethered subsatellite via a longitudinally flexible tether. The infinite-horizon optimal control problem is solved individually through two Legendre pseudospectral algorithms by using a straightforward domain-transformation technique. Each of the algorithms has its merits. The direct method usually enjoys a large region of convergence and the indirect quasi-linear approach is quite easy to implement. A comparison of the numeric results reveals that the controls and system responses obtained by the direct algorithm match the indirect quasi-linear solutions very well, except at the final LGR node. As also indicated in the case studies, the proposed schemes not only effectively suppress the longitudinal vibrations, but also guarantee high precision for achieving the desired final states via the tension control augmented by an out-of-plane thruster. In addition, purely tension-controlled motions can also be stabilized by the presented controller and eventually remain bounded within a safe region. The generality of the controller designs enables one to apply these approaches to other infinite-horizon optimal control problems of nonlinear dynamic systems.

The feasibility of the proposed controllers is shown here in an open-loop arrangement and based on a simplified model, and a preliminary exploration is made about the idea of online trajectory generation. The real-time merits of the presented schemes can be further exploited to design a closed-loop controller based on more advanced control design techniques such as model-predictive control. Another potential extension of this work is the consideration of transverse flexibility of the tether in the system model. Such considerations will increase the complexity of the problem, but make the control scheme more applicable to practical problems.

Acknowledgments

This work was supported in part by the National Natural Science Foundation of China under grants 10372039 and 10672073 and in part by the Innovation Fund for Graduate Students of Nanjing University of Aeronautics and Astronautics.

References

[1] Cosmo, M. L., and Lorenzini, E. C., *Tethers in Space Handbook*, 3rd ed., Smithsonian Astrophysical Observatory, Cambridge, MA, 1997, pp. 2–35.

[2] Kumar, K. D., "Review of Dynamics and Control of Nonelectrodynamic Tethered Satellite Systems," *Journal of Spacecraft and Rockets*, Vol. 43, No. 4, 2006, pp. 705–720. doi:10.2514/1.5479

[3] Rega, G., "Nonlinear Vibrations of Suspended Cables, Part 1: Modeling and Analysis," *Applied Mechanics Reviews*, Vol. 57, No. 6, 2004, pp. 443–478. doi:10.1115/1.1777224

[4] Bainum, P., and Kumar, V. K., "Optimal Control of the Shuttle-Tethered-Subsatellite System," *Acta Astronautica*, Vol. 7, No. 12, 1980, pp. 1333–1348. doi:10.1016/0094-5765(80)90010-7

[5] Williams, P., "Application of Pseudo-spectral Methods for Receding Horizon Control," *Journal of Guidance, Control, and Dynamics*, Vol. 27, No. 2, 2004, pp. 310–314. doi:10.2514/1.5118

[6] Steindl, A., Steiner, W., and Troger, H., "Optimal Control of Retrieval of a Tethered Subsatellite," *IUTAM Symposium on Chaotic Dynamics and Control of Systems and Processes in Mechanics*, Solid Mechanics and Its Applications, Vol. 122, Springer, Dordrecht, The Netherlands, 2005, pp. 441–450.

[7] Jin, D. P., and Hu, H. Y., "Optimal Control of a Tethered Subsatellite of Three Degrees of Freedom," *Nonlinear Dynamics*, Vol. 46, No. 1–2, 2006, pp. 161–178. doi:10.1007/s11071-006-9021-4

[8] Wen, H., Jin, D. P., and Hu, H. Y., "Optimal Feedback Control of the Deployment of a Tethered Subsatellite Subject to Perturbations," *Nonlinear Dynamics*, Vol. 51, No. 4, Mar. 2008, pp. 501–514. doi:10.1007/s11071-007-9240-3

[9] Williams, P., and Trivailo, P., "On the Optimal Deployment and Retrieval of Tethered Satellites," 41st AIAA/ASME/SAE/ASEE Joint Propulsion Conference and Exhibit, Tucson, AZ, AIAA Paper 2005-4291, 2005.

[10] Williams, P., "In-Plane Payload Capture with an Elastic Tether," *Journal of Guidance, Control, and Dynamics*, Vol. 29, No. 4, 2006, pp. 810–821. doi:10.2514/1.17474

[11] Fahroo, F., and Ross, I. M., "Pseudospectral Methods for Infinite-Horizon Nonlinear Optimal Control Problems," *Journal of Guidance, Control, and Dynamics* (accepted for publication).

[12] Ross, I. M., Gong, Q., Fahroo, F., and Kang, W., "Practical Stabilization Through Real-Time Optimal Control," *American Control Conference 2006*, American Automatic Control Council, Evanston, IL, 2006, pp. 304–309.

[13] Lanoix, E. L. M., "A Mathematical Model for Long Term Dynamics of Tethered Satellite Systems," M.Eng. Thesis, McGill Univ., Montreal, 1999, pp. 24–26.

[14] Wächter, A., and Biegler, L. T., "On the Implementation of a Primal-Dual Interior Point Filter Line Search Algorithm for Large-Scale Nonlinear Programming," *Mathematical Programming*, Vol. 106, No. 1, 2006, pp. 25–57. doi:10.1007/s10107-004-0559-y

[15] Davis, T. A., "A Column Pre-Ordering Strategy for the Unsymmetric-Pattern Multifrontal Method," *ACM Transactions on Mathematical Software*, Vol. 30, No. 2, 2004, pp. 165–195. doi:10.1145/992200.992205